

# Phosphate Adsorption on Aluminum-Impregnated Mesoporous Silicates: Surface Structure and Behavior of Adsorbents

EUN WOO SHIN\*<sup>†</sup> AND JAMES S. HAN

USDA Forest Service, Forest Products Laboratory,  
One Gifford Pinchot Drive, Madison, Wisconsin 53726-2398

MIN JANG, SOO-HONG MIN, AND  
JAE KWANG PARK

Department of Civil and Environmental Engineering,  
University of Wisconsin, Madison, Wisconsin 53706

ROGER M. ROWELL

USDA Forest Service, Forest Products Laboratory,  
One Gifford Pinchot Drive, Madison, Wisconsin 53726-2398

Phosphorus from excess fertilizers and detergents ends up washing into lakes, creeks, and rivers. This overabundance of phosphorus causes excessive aquatic plant and algae growth and depletes the dissolved oxygen supply in the water. In this study, aluminum-impregnated mesoporous adsorbents were tested for their ability to remove phosphate from water. The surface structure of the materials was investigated with X-ray diffraction (XRD), a N<sub>2</sub> adsorption–desorption technique, Fourier transform-infrared (FT-IR), and X-ray photoelectron spectroscopy (XPS) to understand the effect of surface properties on the adsorption behavior of phosphate. The mesoporous materials were loaded with Al components by reaction with surface silanol groups. In the adsorption test, the Al-impregnated mesoporous materials showed fast adsorption kinetics as well as high adsorption capacities, compared with activated alumina. The uniform mesopores of the Al-impregnated mesoporous materials caused the diffusion rate in the adsorption process to increase, which in turn caused the fast adsorption kinetics. High phosphate adsorption capacities of the Al-impregnated mesoporous materials were attributed to not only the increase of surface hydroxyl density on Al oxide due to well-dispersed impregnation of Al components but also the decrease in stoichiometry of surface hydroxyl ions to phosphate by the formation of monodentate surface complexes.

## Introduction

Excessive supply of phosphorus from runoff into water bodies such as lakes, rivers, and creeks causes eutrophication, which is the abundance of aquatic plants, growth of algae, and depletion of dissolved oxygen. Methods of removal of phosphorus from water have been studied during the past

decades. Typical removal methods for high concentration of phosphorus consist of biological treatments such as the conventional activated-sludge process, chemical treatments such as precipitation with Al, Fe, and Ca components, or a combination of both treatments (1–3). However, in the case of a low concentration of phosphorus such as in stormwater runoff, biotreatment and precipitation are not effective. Instead, fixed-bed processes using adsorption methods are recommended as the most effective removal processes for low concentrations (4,5).

In the fixed-bed filtration system, selection of an adsorbent is important. Diverse solid materials including red mud, activated alumina, polymeric ligand exchanger, and sand coated with iron and aluminum oxide have been applied as adsorbents (3–7). Recently, mesoporous materials have been used for the removal of toxic chemicals from water because of the merits of high surface area and nanosized regular pores. Thiol-impregnated mesoporous materials showed considerably high sorption capacity for cations such as mercury ions in water (8, 9). Zhao et al. (10) reported that mesoporous silicate materials containing surfactants could eliminate organic pollutants from water. Mesoporous alumina aluminum phosphates have been applied to eliminate herbicides or chlorinated phenols from aqueous solution (11, 12).

In our recent research, metal- (Fe, Al, and Zn) impregnated mesoporous materials were used for the removal of anions from water (13). The adsorption behaviors of phosphate on the metal-impregnated mesoporous materials were found to be different than adsorption on activated alumina. Of several metal-impregnated mesoporous materials, Al-impregnated mesoporous material showed the highest sorption capacity for arsenate removal. The different adsorption behaviors were caused by the different surface properties of the materials. In this study, the adsorption isotherms and kinetics of phosphate adsorption on Al-impregnated mesoporous materials and activated alumina were examined. The surface properties of those materials were investigated through characterization with X-ray diffraction (XRD), Fourier transform-infrared (FT-IR), BET microporosity measurement, and X-ray photoelectron spectroscopy (XPS) to understand the different phosphate adsorption behaviors based on the distinctive surface structure of the adsorbents.

## Materials and Methods

**Materials.** A mesoporous silicate, SBA-15, was prepared according to the procedure described elsewhere (14). An aliquot of 4.0 g of Pluronic P123 (EO<sub>20</sub>PO<sub>70</sub>EO<sub>20</sub>, Aldrich Chemical Co., Milwaukee, WI) was dissolved in 120 g of 2 M HCl solution and 30 g of deionized water. Then, 8.5 g of tetraethyl orthosilicate (TEOS) was added into the homogeneous solution at 308 K. The solution was stirred for 20 h at 308 K and then aged for 24 h at 353 K. The solid product was filtered, washed, and air-dried at room temperature. Calcination was conducted by slowly increasing the temperature from room temperature to 773 K in 14 h and heating at 773 K for 6 h to completely eliminate the surfactants.

Aluminum was impregnated into SBA-15 by the incipient wetness impregnation method. The aqueous solution containing an aluminum precursor, aluminum nitrate nonahydrate (Al(NO<sub>3</sub>)<sub>3</sub>·9(H<sub>2</sub>O), Aldrich Chemical Co.), was dropped into SBA-15. After impregnation, the samples were dried at room temperature in a hood for 1 day and then oxidized at 673 K for 4 h in air. The amount of aluminum loaded into SBA-15 was controlled by dissolving different amounts of aluminum precursor into the same amount of deionized

\* Corresponding author phone: (608) 262-0614; fax: (608) 262-1228; e-mail: eshin90@yahoo.com or ewshin@wisc.edu.

<sup>†</sup> Present address: Dept. of Biological Systems Engineering, University of Wisconsin–Madison, 460 Henry Mall, Madison, WI 53706.

TABLE 1. Summary of Properties of Prepared Samples

| samples                 | Al-impregnation amount (%) | Al/Si | d spacing (nm) | a <sub>0</sub> (nm) |
|-------------------------|----------------------------|-------|----------------|---------------------|
| activated alumina       |                            |       |                |                     |
| SBA-15                  | 0                          | 0     | 10.75          | 12.41               |
| Al <sub>5</sub> SBA-15  | 5                          | 0.11  | 10.18          | 11.75               |
| Al <sub>10</sub> SBA-15 | 10                         | 0.22  | 9.67           | 11.16               |
| Al <sub>30</sub> SBA-15 | 30                         | 0.66  | 10.75          | 12.41               |

water. The activated alumina used in this study was also acquired from Aldrich Chemical Co. The surface area and the average pore diameter of activated alumina were 155 m<sup>2</sup>/g and 5.9 nm, respectively. Physical properties of the samples used in this study are summarized in Table 1.

**Surface Analysis.** X-ray diffraction (XRD) patterns of the prepared samples were acquired with a Stoe high-resolution X-ray diffractometer (Microphotonics, Allentown, PA) using Cu K $\alpha$  radiation (40 kV, 25 mA) of wavelength 0.154 nm to confirm the structure of the mesoporous materials. All XRD patterns were obtained from 0.8° to 3.0° with a scan speed of 0.2°/min. The XPS experiments were conducted with a Perkin-Elmer (Norwalk, CT) 5400 ESCA spectrometer under 10<sup>-8</sup> Torr of vacuum condition to compare the chemical state of the elements loaded into all samples. Mg K $\alpha$  radiation was used as an X-ray source.

The IR spectra of each sample were recorded on a Mattson Galaxy 5020 (Mattson Instruments, Madison, WI) to check the change in the functional group of the oxide surface after Al impregnation. All the samples were mixed with KBr, compacted in a uniaxial press under a nominal pressure of 1 GPa, and measured at room temperature. The BET surface area and the pore size distributions of each sample were measured by the N<sub>2</sub> adsorption-desorption technique using a Micromeritics (Norcross, GA) ASAP 2000 analyzer. Degassing of the samples was conducted at 523 K for 1 day.

**Phosphate Adsorption Test.** Phosphate isotherms for the samples were acquired through batch experiments. Before adsorption experiments, the samples were washed with deionized water and dried at room temperature overnight. Solid samples weighing between 0.01 and 0.4 g were placed in 125-mL bottles with 100 mL of solution that had 10 ppm phosphorus concentration. Sodium dihydrogenphosphate (NaH<sub>2</sub>PO<sub>4</sub>, Aldrich Chemical Co.) was used as the phosphorus source. The ionic strength of the solutions was maintained at 0.01 M using NaNO<sub>3</sub>. The sealed sample bottles were placed in a shaker and shaken at 200 rpm at room temperature. After shaking the sample bottles for 3 h, the pH of the solutions was adjusted to 6.4 through the addition of either acid (HNO<sub>3</sub>, 0.1 M) or base (NaOH, 0.1 M) stock solution. Then, all the sample bottles were placed again in a shaker for 48 h at room temperature. The final pH of the solutions ranged from 6.7 to 7.2, depending on the amount and the sort of solid samples. After shaking, the suspension was filtered immediately with a 0.45- $\mu$ m microfilter. The phosphorus concentration of the filtered solutions was analyzed by an inductively coupled plasma atomic emission spectrometer (Ultima ICP-AES, Jobin Yvon, Inc., Edison, NJ).

The Langmuir isotherm model was applied to the isotherm data. The Langmuir isotherm is

$$q_e = \frac{bQ_{\max}C_e}{1 + bC_e} \quad (1)$$

where  $q_e$  is amount adsorbed at equilibrium (mg/g),  $b$  is the Langmuir constant (L/g),  $Q_{\max}$  is maximum adsorbate adsorption amount (grams adsorbate/grams adsorbent), and  $C_e$  is phosphorus concentration at equilibrium.

Adsorption kinetic experiments were performed in 1-L solutions with 0.4 g of sample powders. The initial phosphorus

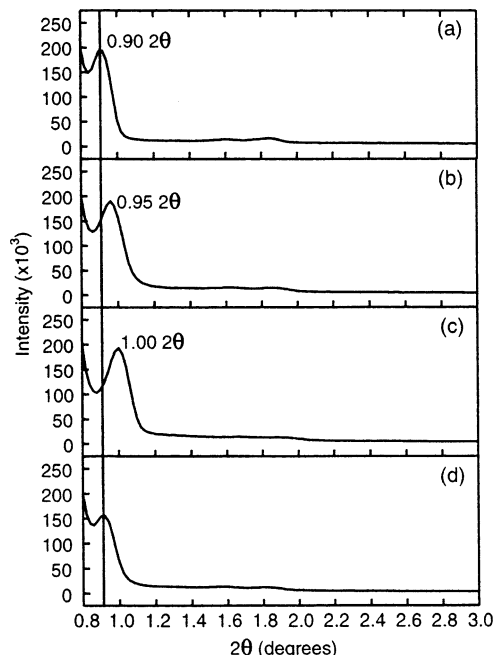


FIGURE 1. X-ray diffraction patterns of each sample: (a) SBA-15, (b) Al<sub>5</sub>SBA-15, (c) Al<sub>10</sub>SBA-15, and (d) Al<sub>30</sub>SBA-15.

concentration of the solution was 10 mg/L, and the pH of the solution was maintained at 6.4. The suspension was stirred by a magnetic bar, and the supernatant samples were taken at various times during a 3-h experiment. Also, the phosphorus concentrations of these samples were measured with an inductively coupled plasma atomic emission spectrometer.

All kinetic data were fitted to the pseudo-second-order kinetic model suggested by Ho and McKay (15). The kinetic rate equations can be written as follows

$$\frac{dq_t}{dt} = k(q_e - q_t)^2 \quad (2)$$

where  $q_t$  is the amount adsorbed at time  $t$  (mg/g) and  $k$  is the equilibrium rate constant of the second-order sorption (g/mg·min). Nonlinear regressions using a least-squares fitting program (Origin 7.0, OriginLab Corp., Northampton, MA) were conducted to acquire the best estimate of all constants for all the models.

## Results and Discussion

**Surface Structure. X-ray Diffraction.** The XRD patterns of SBA-15 and Al-impregnated SBA-15 are shown in Figure 1. The main peak appears at 0.9 of  $2\theta$ , and two small peaks appear at 1.6 and 1.8, respectively, which match well with the patterns of SBA-15 in previous studies (14, 16) (Figure 1a). This confirms successful synthesis of SBA-15 silicate. The peaks can be indexed as (100), (110), and (200), and the  $d$  spacing value as well as the unit cell parameter ( $a_0$ ) for the intense (100) peak can be calculated through Bragg's law. Those values for each sample are listed in Table 1. Addition

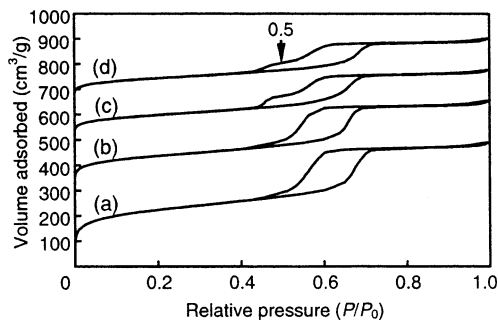


FIGURE 2. Nitrogen adsorption-desorption isotherms for each sample: (a) SBA-15, (b) Al<sub>5</sub>SBA-15, (c) Al<sub>10</sub>SBA-15, and (d) Al<sub>30</sub>SBA-15.

TABLE 2. Pore Structure Parameters of Samples Calculated from the Desorption Branch of N<sub>2</sub> Adsorption Isotherm

| samples                 | A <sub>BET</sub> (m <sup>2</sup> /g) <sup>a</sup> | A <sub>BJH</sub> (m <sup>2</sup> /g) <sup>a</sup> | D <sub>BJH</sub> (nm) <sup>a</sup> |
|-------------------------|---|---|------------------------------------|
| activated alumina       | 155 <sup>b</sup>                                  |   | 5.9 <sup>b</sup>                   |
| SBA-15                  | 768   | 554   | 4.79                               |
| Al <sub>5</sub> SBA-15  | 476   | 489   | 4.82                               |
| Al <sub>10</sub> SBA-15 | 343   | 412   | 4.32                               |
| Al <sub>30</sub> SBA-15 | 328   | 369   | 4.42                               |

<sup>a</sup> A, surface area; D, diameter; BET, Brunauer, Emmett, and Teller; BJH, Barrett, Joyner, and Halenda. <sup>b</sup> Data from Aldrich Chemical Co.

of the Al component reduced the unit cell size ( $a_0$ ) or destroyed the crystallinity of mesoporous silicates. Up to 10% (wt) Al impregnation, the unit cell size of mesoporous silicates became smaller and the remaining crystallinity was unchanged. The positions of the (100) peak shifted from 0.9 to 1.0 with increasing the amount of Al, whereas the peak intensities were almost the same. According to Romero et al. (17), the peak shift represents the contraction of unit cell due to the substitution of the silicon by aluminum. However, in the case of Al<sub>30</sub>SBA-15, the peak remained at the same position while the peak intensity decreased, indicating that the crystallinity was destroyed. Those results are consistent with the results of FT-IR (see next sections) in this study and the finding that the addition of Al to MCM-41 reduced the pore size and crystallinity of MCM-41 (10). The destruction of pore structure caused the decrease of adsorption capacity of the sample because adsorbates could not access the adsorption sites inside the blocked pores.

**Nitrogen Adsorption.** Nitrogen adsorption isotherms of all the samples are shown in Figure 2. All the patterns showed typical irreversible type IV adsorption isotherms with a H1 hysteresis loop as defined by IUPAC (18). In the isotherms of SBA-15 and Al<sub>5</sub>SBA-15 (Figure 2a and b), the volumes adsorbed inflected sharply in the range between 0.5 and 0.7 of relative pressure ( $P/P_0$ ). The sharpness of these steps implied that the mesopores of those samples were uniform. In contrast, for Al<sub>10</sub>SBA-15 and Al<sub>30</sub>SBA-15, shoulders were observed in the desorption branch of the hysteresis loop, indicating that those samples had mesopores of two different sizes, affected by Al impregnation.

The calculated BET surface areas and the mesopore parameters based on the Barrett, Joyner, and Halenda (BJH) analysis are shown in Table 2. Both BET surface areas ( $A_{BET}$ ) and mesopore surface areas ( $A_{BJH}$ ) decreased with the amount of added Al components. However, in Table 2, the average pore diameters  $D_{BJH}$  decreased from about 4.8 to 4.4 nm above 10% of Al impregnation, whereas they seemed constant up to 5% of Al impregnation. Accordingly, up to 5% of Al impregnation, added Al components induced the reduction of surface areas of the samples, whereas the mesopore structures of the samples were affected by Al components above 10% of Al impregnation.

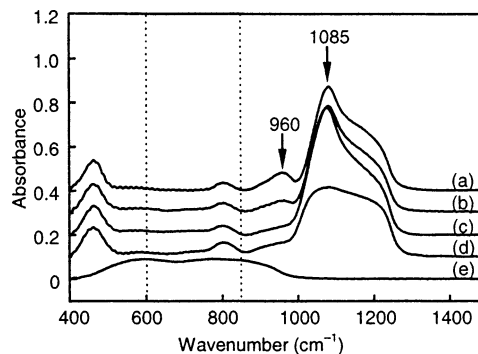


FIGURE 3. Infrared spectra of each sample: (a) SBA-15, (b) Al<sub>5</sub>SBA-15, (c) Al<sub>10</sub>SBA-15, and (d) Al<sub>30</sub>SBA-15, and (e) activated alumina.

**Infrared Spectra.** Figure 3 shows the FT-IR spectra of each sample. In the IR pattern of SBA-15 (Figure 3a), the three peaks at 465, 800, and 1085 cm<sup>-1</sup> correspond to rocking, bending (or symmetric stretching), and asymmetric stretching of the intertetrahedral oxygen atoms in the SiO<sub>2</sub> structure (19). The peak at 960 cm<sup>-1</sup> is also assigned to the stretching of nonbridging oxygen atoms, for example, Si-OH. Added Al components weakened both the peak intensities of 960 and 1085 cm<sup>-1</sup>. However, the change in intensity of each peak appeared different according to Al impregnation amount. The peak at 960 cm<sup>-1</sup> decreased proportionally up to 10% of Al impregnation and remained the same intensity above 10% of Al impregnation, while the intensity of the peak at 1085 cm<sup>-1</sup> decreased dramatically only at Al<sub>30</sub>SBA-15. Since the peak at 960 cm<sup>-1</sup> originated from the silanol group in the framework of SBA-15, the gradual decrease of this peak at Al<sub>5</sub>SBA-15 and Al<sub>10</sub>SBA-15 was attributed to the interaction between the silanol group in SBA-15 and the added Al components during the impregnation process. The amount of the silanol group in SBA-15 that can react with Al components was confined, so that the silanol group in SBA-15 was almost consumed when 10% of the Al component was impregnated. In the case of Al<sub>30</sub>SBA-15, the Al components impregnated excessively into SBA-15 seemed to attack the Si-O bonding in the mesoporous framework as the peak at 1085 cm<sup>-1</sup> lessened rapidly. It might be interpreted that the excessive Al components destroyed the pore structure of SBA-15, which was supported by XRD results. Consequently, Al components were incorporated into SBA-15 by reaction with the silanol functional group of SBA-15 framework, and extra Al components ruined the pore structure of SBA-15.

Even though the IR pattern of activated alumina shown in Figure 3e appeared to consist of two broad peaks around 600 and 850 cm<sup>-1</sup>, several IR bands of alumina were covered under those broad peaks. According to Pecharroman et al. (20), above 400 cm<sup>-1</sup>, three IR bands (around 600, 770, and 850 cm<sup>-1</sup>) can be assigned to the bending of oxygen against aluminum ions, stretching of anions against octahedral cations, and stretching of anions against octahedral and tetrahedral cations, correspondingly. In the interpretation of their electron energy loss spectroscopy (EELS) results, Crowell et al. (21) postulated that the peak around 600 cm<sup>-1</sup> was connected with a vertical motion of the oxygen overlayer and the surface Al and the peak around 850 cm<sup>-1</sup> mode was attributed to a similar motion by the oxygen underlayer and the subsurface Al. However, no matter what the assignments of the IR peaks of the alumina were, IR patterns of Al-impregnated SBA-15 were almost the same as those of SBA-15. Even in the IR pattern of Al<sub>30</sub>SBA-15 where the most Al components were impregnated, characteristic IR peaks of alumina did not appear at all. Nonetheless, from the results of XRD, BET N<sub>2</sub> adsorption, and FT-IR, the interaction between impregnated Al components and SBA-15 is clear. Furthermore, in the XPS results described in the next section,

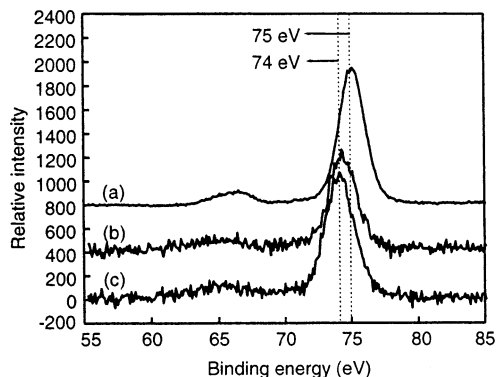


FIGURE 4. X-ray photoelectron spectroscopy of Al 2p: (a) activated alumina, (b) Al<sub>10</sub>SBA-15, and (c) Al<sub>30</sub>SBA-15.

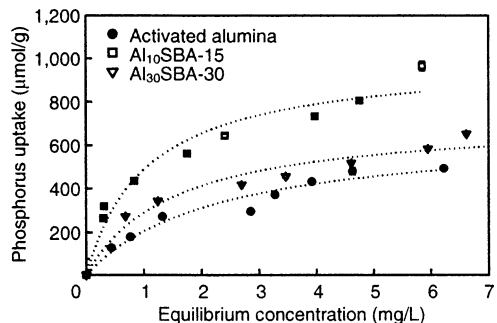


FIGURE 5. Phosphate adsorption isotherms on each sample with the results fitted to the Langmuir equation.

TABLE 3. Al 2p Binding Energies and Full-Width Half-Maximum (fwhm) of Each Sample

| sample                  | Al 2p               |           |
|-------------------------|---------------------|-----------|
|                         | binding energy (eV) | fwhm (eV) |
| activated alumina       | 75.0                | 1.99      |
| Al <sub>10</sub> SBA-15 | 74.1                | 2.06      |
| Al <sub>30</sub> SBA-15 | 74.0                | 2.15      |

the peak of Al 2p was obvious. Therefore, the Al phase exists in Al-impregnated SBA-15 despite no detection of the Al phase by FT-IR.

**X-ray Photoelectron Spectroscopy.** The XPS of Al 2p on each sample is shown in Figure 4. The XPS results were corrected by C 1s peak and fitted to a Gaussian curve to determine peak width. The binding energies and the full-width half-maximums (fwhm) of Al 2p for each sample are summarized in Table 3. The binding energy of activated alumina is 75.0 eV. In the case of Al-impregnated SBA-15, the binding energies shifted to 74.0 or 74.1 eV by 1 eV, which implies that the Al phase in SBA-15 might be different from activated alumina. Because the binding energy of Al metal appears generally around 72 eV and those of the oxides are between 73.5 and 75.5 eV (22–27), the Al phase of Al-impregnated SBA-15 did not appear to be metal. In the results of oxidation on Al single crystal, a clue for the Al phase of Al-impregnated samples can be inferred. McConville et al. (23) found that the chemical states of Al–O during oxidation of Al(111) were diverse by the chemical shift of Al 2p in XPS results. According to Pashutski et al. (25), three binding energies of Al 2p, 73.0, 74.5, and 75.4 eV, in study of O<sub>2</sub> adsorption on Al(100), were assigned to pure Al, Al<sub>x</sub>O<sub>y</sub> ( $x/y = 3:1$  or  $1:1$ ), and Al<sub>2</sub>O<sub>3</sub>, correspondingly. Accordingly, the value of 74.0 eV for binding energy in Figure 5 indicates that the Al phase of Al-impregnated SBA-15 can be assigned to AlO, which is less oxidized than Al<sub>2</sub>O<sub>3</sub>. The Al components anchored inside SBA-15 by the reaction with silanol group

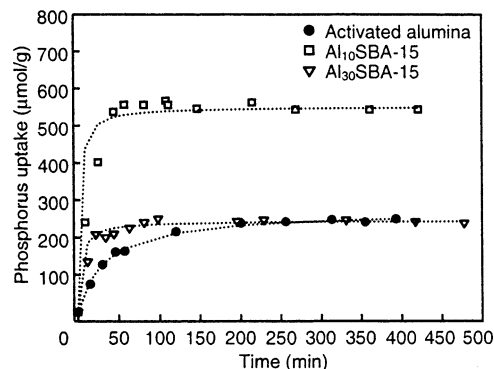


FIGURE 6. Adsorption kinetics of phosphate on each sample.

TABLE 4. Langmuir Parameters for Each Sample

| samples                 | Langmuir <sup>a</sup> |         |                           |        |
|-------------------------|-----------------------|---------|---------------------------|--------|
|                         | R <sup>2</sup>        | b (L/g) | Q <sub>max</sub> (μmol/g) | P/Al   |
| activated alumina       | 0.934                 | 0.43    | 565                       | 0.0288 |
| Al <sub>10</sub> SBA-15 | 0.954                 | 0.95    | 862                       | 0.231  |
| Al <sub>30</sub> SBA-15 | 0.960                 | 0.66    | 619                       | 0.0556 |

<sup>a</sup> b is Langmuir constant; Q<sub>max</sub> is maximum adsorbate adsorption amount.

were oxidized through the calcination step. However, it is believed that the aluminum oxide formed in Al-impregnated SBA-15 might be at a different oxidation state than activated alumina.

**Phosphate Adsorption Behavior. Adsorption Isotherm.** Phosphate isotherms for each sample and fitting results are shown in Figure 5 and Table 4. Although the phosphate isotherm test was performed with SBA-15 samples, SBA-15 did not adsorb phosphates in measurable quantities. Because of this, it can be said that the SBA-15 itself did not trap phosphate. As shown in the isotherms, Al-impregnated SBA-15 had higher sorption capacities for phosphate than activated alumina. Al<sub>10</sub>SBA-15 adsorbed more phosphate than Al<sub>30</sub>SBA-15 even though the latter had a larger Al content than the former. These results are quantitatively shown in the Langmuir parameters in Table 4. The Q<sub>max</sub> of activated alumina, Al<sub>30</sub>SBA-15, and Al<sub>10</sub>SBA-15 was 565, 619, and 862 μmol/g, respectively. The important values in this experiment are the phosphate sorption capacities based on Al amount in each adsorbent, which are expressed as P/Al in Table 4. The mole ratio of phosphorus adsorbed of each sample in Table 4, P/Al of Al<sub>10</sub>SBA-15, was 0.231 on molar aluminum base, almost eight times higher than 0.0288, which is that of activated alumina. In the case of Al<sub>30</sub>SBA-15, P/Al was 0.0556, two times higher than activated alumina. Accordingly, it can be concluded that Al-impregnated SBA-15 demonstrate more active adsorption sites for phosphorus per aluminum than activated alumina, and those active sites of Al-impregnated mesoporous materials depend on the Al impregnation amount. Despite the larger Al-impregnated amount, Al<sub>30</sub>SBA-15 had fewer active sites for phosphorus than Al<sub>10</sub>SBA-15 due to destruction of pore structure.

**Adsorption Kinetics.** Figure 6 shows the kinetic results of phosphorus adsorption on each sample. The results were fitted to a pseudo-second-order eq 2. The kinetic parameters acquired from fitting results are summarized in Table 5. The high determination coefficients (R<sup>2</sup>) for a pseudo-second-order equation for every sample implied that the adsorption of phosphate on those samples was closer to chemisorption (15). Interestingly, there was remarkable difference in adsorption rates between activated alumina and Al-impregnated mesoporous materials. Activated alumina reached

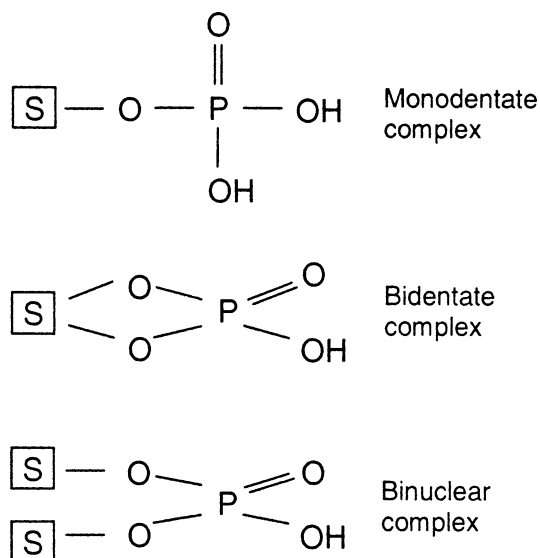


FIGURE 7. Possible configurations of the phosphate surface complexes (33).

TABLE 5. Kinetic Parameters for Phosphorus Adsorption on Each Sample<sup>a</sup>

| samples                 | $k$ (g/ $\mu$ mol·min) | $q_e$ ( $\mu$ mol/g) | $R^2$ |
|-------------------------|------------------------|----------------------|-------|
| activated alumina       | 0.0844                 | 347                  | 0.998 |
| Al <sub>10</sub> SBA-15 | 0.599                  | 710                  | 0.998 |
| Al <sub>30</sub> SBA-15 | 0.826                  | 315                  | 0.999 |

<sup>a</sup>  $k$  is equilibrium rate constant of the second-order sorption;  $q_e$  is amount adsorbed at equilibrium.

equilibrium after 4 h kinetic time while Al-impregnated SBA-15 did so within 1 h (Figure 7). Quantitative results are shown in Table 5. The rate constants ( $k$ ) of Al-impregnated SBA-15 at 0.599 and 0.826 g/ $\mu$ mol·min were much greater than that of activated alumina at 0.0844 g/ $\mu$ mol·min, which means that adsorption of phosphate on Al-impregnated SBA-15 occurred much faster than on activated alumina. In addition, the adsorption capacities obtained from kinetic results, 710, 347, and 315  $\mu$ mol/g for Al<sub>10</sub>SBA-15, activated alumina, and Al<sub>30</sub>SBA-15, respectively, were consistent with the results from isotherms.

**Surface Structure of Adsorbents Compared with Adsorption Behaviors.** The distinctive adsorption behaviors of Al-impregnated mesoporous materials—fast kinetics and high adsorption capacities—were investigated in terms of physical and chemical properties of the adsorbents: pore structures of porous materials and surface structures of Al oxide. In the adsorption process, the former is closely connected with the accessibility of adsorbents to adsorption sites while the latter affects the surface reaction of adsorbents.

Compared with activated alumina, Al-impregnated SBA-15 showed the fast kinetics in phosphate adsorption. This fast sorption ability can be attributed to the physical property of Al-impregnated SBA-15. The porosities of both Al-impregnated SBA-15 and activated alumina are developed so well that the adsorption kinetics may be controlled by diffusion rate. However, the diffusion of molecules inside pores shows different trends caused by different pore structures of each adsorbent. The pore structure of Al-impregnated SBA-15 is composed of hexagonal open pores of the MCM-41 type, which has a relatively uniform mesopore size excluding macropore structures (14). The open and homogeneous mesopore structure of Al-impregnated SBA-15 improved the accessibility of molecular species to adsorption sites (28). Activated alumina are amorphous

matrices of aluminum oxides containing diverse pores that range from micro to macro with bottleneck shapes of pore structures (29). This feature can hinder the accessibility of phosphate molecules to the adsorption sites of activated alumina and retard the adsorption processes on the whole. In other words, the diffusion limitation due to the bottleneck shape of pore structures enables the adsorption process in activated alumina to be slow compared with Al-impregnated SBA-15 containing uniform mesopore size, even though the average pore size of activated alumina was bigger than that of Al-impregnated SBA-15.

The damage of the pore structure has an immediate effect on the capacity of the materials by influencing the accessibility to adsorption sites by adsorbates. For example, the adsorption capacity of Al<sub>30</sub>SBA-15, in which part of the pore structure was ruined, decreased compared with Al<sub>10</sub>SBA-15 because the adsorption sites inside the ruined pore became inactive to adsorption. In the case of Al<sub>30</sub>SBA-15, as shown in the results of XRD and FT-IR, excessive Al attacked the silicate in the framework of the mesoporous material and as a result the mesopore structures were partially demolished.

Meanwhile, Al<sub>10</sub>SBA-15, whose pore structure was not damaged by Al impregnation, showed greater adsorption capacity than activated alumina. Moreover, the amount of phosphate adsorbed per alumina of Al<sub>10</sub>SBA-15 was much greater than that of activated alumina, which implies that relatively more adsorption sites on the surface were exposed to adsorbates in the case of Al<sub>10</sub>SBA-15. The FT-IR results showed that the loaded Al components reacted selectively with the Si-OH group of the mesoporous framework. The selective reaction resulted in a well-coated aluminum oxide inside SBA-15. On this basis, we believe this selective deposition improved the adsorption capacity of Al<sub>10</sub>SBA-15 by increasing the number of adsorption sites exposed to adsorbates. This idea is supported by other studies of the same materials (30). Potentiometric titration and modeling using surface complexation theory were conducted to quantify the amount of the surface hydroxyl group. The results showed that Al<sub>10</sub>SBA-15 had 5.7 times more site density and 2.5 times more surface hydroxyl groups than activated alumina. Consequently, the higher surface hydroxyl density on aluminum oxide was accomplished by the Al impregnation onto SBA-15.

On the other hand, differences in the surface structure of aluminum oxide might affect the surface reactions of phosphate on the adsorbents. Phosphate is specifically adsorbed on inorganic materials by a ligand-exchange mechanism with a reactive surface hydroxyl ion (31–34). There are three possible phosphate surface complexes resulting from the ligand exchange reaction: binuclear, bidentate, and monodentate complexes (Figure 7) (33). From the quantitative relationship between hydroxyl ion release and phosphate adsorption, Rajan (35) proposed that phosphate adsorbs on hydrous alumina to form both monodentate and binuclear complexes, depending on the phosphate concentration. Furthermore, the mono- and bidentate surface complexes have been used to explain the reaction step in anion adsorption by metal hydroxide (36–39). The reaction mechanism consists of two steps: forming monodentate surface complexes (step I) and then bidentate surface complexes (step II). As shown in Figure 7, in the monodentate surface complex of step I, phosphate adsorbed to the surface hydroxyl ion with one coordination number. The bidentate surface complex, however, was bound to two surface hydroxyl ions, needing double-coordinated adsorption sites.

In this study, it was postulated that the configuration of phosphate surface complexes was affected by the surface structure of aluminum oxide. The results of FT-IR and XPS showed that Al-impregnated SBA-15 had less oxidized alumina such as AlO than did activated alumina, implying

that the surface structure of alumina in Al-impregnated SBA-15 is favorable to form the monodentate surface complex because of low coordination numbers of aluminum oxide. In other words, the distinctive aluminum oxide structure of Al-impregnated SBA-15 was thought to inhibit the formation of the bidentate surface complex on Al-impregnated SBA-15. In other studies using the same adsorbents, mono- and bidentate surface densities were obtained from surface complexation modeling (The computer program FITEQL 4.0) on the arsenate removal from water by activated alumina and Al-impregnated SBA-15 (32). The ratios of monodentate to bidentate surface complexes for activated alumina and Al<sub>10</sub>SBA-15 were 0.549 and 1.29, respectively. The oxide surface of Al<sub>10</sub>SBA-15 was covered mainly with monodentate surface complexes at equilibrium, whereas bidentate surface complexes were prevalent on the surface of activated alumina.

The high portion of monodentate surface complexes during the adsorption process additionally explains the increase of adsorption capacity on Al-impregnated SBA-15. When monodentate surface complexes are formed, the stoichiometry between phosphates and surface hydroxyl ions is one to one, while phosphate reacts with two surface hydroxyl ions of aluminum oxide in bidentate surface complexes. Accordingly, monodentate adsorption is more efficient in the removal of phosphate from water.

### Acknowledgments

The authors thank the USDA Forest Service Large-Scale Watershed Restoration Project—New York City Watershed Study and the USDA Forest Service National Fire Funding for financial support. The use of trade or firm names in this publication is for reader information and does not imply endorsement by the U.S. Department of Agriculture of any product or service. The Forest Products Laboratory is maintained in cooperation with the University of Wisconsin.

### Literature Cited

- (1) Donnert, D.; Salecker, M. *Water Sci. Technol.* **1999**, *40*, 195–202.
- (2) Jenkins, D.; Ferguson, J. F.; Menar, A. B. *Water Res.* **1971**, *5*, 369–389.
- (3) Ayoub, G. M.; Koopman, B.; Pandya, N. *Water Environ. Res.* **2001**, *73*, 478–485.
- (4) Hano, T.; Takanashi, H.; Hirata, M.; Urano, K.; Eto, S. *Water Sci. Technol.* **1997**, *35*, 39–46.
- (5) Zhao, D. Y.; Sengupta, A. K. *Water Res.* **1998**, *32*, 1613–1625.
- (6) Akay, G.; Keskinler, B.; Cakich, A.; Danis, U. *Water Res.* **1998**, *32*, 717–726.
- (7) Lo, S.-L.; Jeng, H.-T.; Lai, C.-H. *Water Sci. Technol.* **1997**, *35*, 63–70.
- (8) Merchier, L.; Pinnavaia, T. J. *Environ. Sci. Technol.* **1998**, *32*, 2749–2754.
- (9) Feng, X.; Fryxell, G. E.; Wang, L.-Q.; Kim, A. Y.; Liu, J.; Kemner, K. M. *Science* **1997**, *276*, 923–926.
- (10) Zhao, H.; Nagy, K. L.; Waples, J. W.; Vance, G. F. *Environ. Sci. Technol.* **2000**, *34*, 4822–4827.
- (11) Danis, T. G.; Albanis, T. A.; Petrakis, D. E.; Pomonis, P. J. *Water Res.* **1998**, *32*, 295–302.
- (12) Konstantinou, I. K.; Albanis, T. A.; Petrakis, D. E.; Pomonis, P. J. *Water Res.* **2000**, *34*, 3123–3136.
- (13) Jang, M.; Shin, E. W.; Park, J. K. *The Proceedings of the WEFTEC02 meetings*; The Water Environment Federation: Chicago, IL, 2002.
- (14) Zhao, D.; Feng, J.; Huo, Q.; Melosh, N.; Fredrickson, G. H.; Chmelka, B. F.; Stucky, G. D. *Science* **1998**, *279*, 548–552.
- (15) Ho, Y. S.; McKay, G. *Water Res.* **2000**, *34*, 735–742.
- (16) Luan, Z. H.; Maes, E. M.; van der Heide, P. A. W.; Zhao, D. Y.; Czernuszewicz, R. S.; Kevan, L. *Chem. Mater.* **1999**, *11*, 3680–3686.
- (17) Romero, A. A.; Alba, M. D.; Klinowski, J. *J. Phys. Chem. B* **1998**, *102*, 123–128.
- (18) Sing, K. S. W.; Everett, D. H.; Haul, R. A. W.; Moscow, L.; Pierotti, R. A.; Rouquerol, J.; Siemieniewska, T. *Pure Appl. Chem.* **1985**, *57*, 603.
- (19) Primeau, M.; Vautey, C.; Langlet, M. *Thin Solid Films* **1997**, *310*, 47–56.
- (20) Pecharrroman, C.; Sobrados, I.; Iglesias, J. E.; Gonzalez-Carreno, T.; Sanz, J. *J. Phys. Chem. B* **1999**, *103*, 6160–6170.
- (21) Crowell, J. E.; Chen, J. G.; Yates, J. T. *Surf. Sci.* **1986**, *165*, 37–64.
- (22) Bose, O.; Kemnitz, E.; Lippitz, A.; Unger, W. E. S. *Fresenius J. Anal. Chem.* **1997**, *358*, 175–179.
- (23) McConville, C. F.; Seymeour, D. L.; Woodruff, D. P.; Bao, S. *Surf. Sci.* **1987**, *188*, 1–14.
- (24) Ocal, C.; Basurco, B.; Ferrer, S. *Surf. Sci.* **1985**, *157*, 233–243.
- (25) Pashutski, A.; Hoffman, A.; Folman, M. *Surf. Sci.* **1989**, *208*, L91–L97.
- (26) Rotole, J. A.; Sherwood, P. M. A. *J. Vac. Sci. Technol. A* **1999**, *17*, 1091–1096.
- (27) Thomas, S.; Sherwood, P. M. A. *Anal. Chem.* **1992**, *54*, 2488–2495.
- (28) Burleigh, M. C.; Markowitz, M. A.; Spector, M. S.; Gaber, B. P. *Chem. Mater.* **2001**, *13*, 4760–4766.
- (29) Kim, Y. S. *Kor. J. Mater. Res.* **2001**, *11*, 957–965.
- (30) Jang, M.; Shin, E. W.; Park, J. K.; Choi, S. I. *Environ. Sci. Technol.* **2003**, *37*, 5062–5070.
- (31) Sparks, D. L. *Environmental Soil Chemistry*, 2nd ed.; Academic Press: San Diego, CA, 2003; p 176.
- (32) He, L. M.; Zelazny, L. W.; Baligar, V. C.; Ritchey, K. D.; Martens, D. C. *Soil Sci. Soc. Am. J.* **1997**, *61*, 784–793.
- (33) Goldberg, S.; Sposito, G. *Commun. Soil Sci. Plant Anal.* **1985**, *16*, 801–821.
- (34) Sposito, G. *The Chemistry of Soils*; Oxford University Press: New York, 1989; p 157.
- (35) Rajan, S. S. S. *Nature* **1975**, *253*, 434–436.
- (36) *The Nature and Properties of Soils*, 12th ed.; Brady, N. C., Weil, R. R., Eds.; Prentice Hall: Upper Saddle River, NJ, 1999; p 560.
- (37) Grossl, P. R.; Eick, M.; Sparks, D. L.; Goldberg, S.; Ainsworth, C. C. *Environ. Sci. Technol.* **1997**, *31*, 321–326.
- (38) Fendorf, S.; Eick, M. J.; Grossl, P.; Sparks, D. L. *Environ. Sci. Technol.* **1997**, *31*, 315–320.
- (39) Kafkafi, U.; Posner, A. M.; Quirk, J. P. *Soil Sci. Soc. Am. Proc.* **1967**, *31*, 348–353.

Received for review May 29, 2003. Revised manuscript received October 9, 2003. Accepted November 4, 2003.

ES030488E